JOURNAL OF SOLID STATE CHEMISTRY 44, 230–244 (1982)

Nonstoichiometry and Defects in V_2O_3

NOBUO OTSUKA, HIROSHI SATO, G. L. LIEDL, AND J. M. HONIG*

School of Materials Engineering, Purdue University, West Lafayette, Indiana 47907

Received February 4, 1982; in final form April 16, 1982

The structural mechanism which accommodates nonstoichiometry in V_2O_3 was investigated by transmission electron microscopy. The existence of distinct diffuse scattering was observed as the boundary of the homogeneity range was approached. The analysis of the diffuse scattering indicates the formation of one-dimensional microdomains in the c direction having a structure similar to VO_2. Orientation relations between V_2O_3 and V_3O_5 (which is formed from V_2O_3 by heat treatment in an oxidizing atmosphere) show that V_3O_5 is formed by redistribution of vanadium ions among the octahedral interstitial sites of common close-packed sublattice consisting of oxygen ions. Possible relations between the present observations and physical properties in nonstoichiometric V_2O_{3+x} are discussed.

Introduction

The physical properties, as well as the phase diagram of the V–O system near V_2O_3 have been well investigated because of the existence of the metal–insulator (M–I) transition in V_2O_3 (*1–3*). At the stoichiometric composition, the M–I transition temperature is about 170K, but it decreases rapidly with excess oxygen content and vanishes at around $V_2O_{3.027}$. Nonstoichiometry in oxides is known to be generally compensated by some kind of structural defects. Therefore, such a rapid change of properties of V_2O_3 with the excess oxygen content raises a question whether a specific structural form of nonstoichiometry in V_2O_3 is responsible for the suppression of the antiferromagnetic insulating phase.

Extensive studies of such structural defects related to nonstoichiometry in transition metal oxides have been made in oxides with the rock salt structure, such as TiO, VO, and FeO (*4–10*). Most of these oxides show wide homogeneity ranges, and point defects (vacancies in metal ion sites) created by excess oxygen content have been found to form ordered arrangements at low temperatures, and, near the order–disorder transition points, extensive diffuse scattering appears as a result of the clustering of point defects. In V_2O_3, on the other hand, the homogeneity range, which approximately extends to $V_2O_{3.08}$, is so narrow that a detailed study of possible clustering of point defects, if any, has been lacking. Even the existence of diffuse scattering in the homogeneity range of V_2O_3 has not been reported.

Structures of transition metal oxides can be regarded as ordered distributions of metal ions among interstitial sites of the close-packed lattice of oxygen ions if distortions are disregarded, and different phases can then be regarded to be different

* Department of Chemistry, Purdue University.

0022-4596/82/110230–15$02.00/0

ordered distributions of metal ions in interstitial sites of the common oxygen close-packed lattice. In V_2O_3, only two-thirds of the available octahedral sites of the hexagonal closed-packed oxygen lattice are occupied. With this low occupancy, the local metal ion distribution around an oxygen ion can be very sensitively affected with the additional vacant sites created by nonstoichiometry due to the freedom in the rearrangement. Therefore, even a small degree of nonstoichiometry in V_2O_3 can introduce more clustering compared to the case of VO in which all octahedral sites of the cubic closed-packed lattice of oxygen ions are occupied by metal ions. In the following, a detailed account is given of our effort to investigate the structural defects associated with nonstoichiometry in V_2O_3.

Experimental Procedure

Specimens of six different compositions were chosen to cover the whole homogeneity range and the two-phase region near the boundary. These are listed in Table I. These specimens were prepared at the Central Materials Preparation Facility at Purdue University; details of the preparation method are given elsewhere (*3*). First, V_2O_5 powder (Cerac, 99.9%) was reduced to V_2O_3 in a hydrogen atmosphere at 1000°C. Single crystals of V_2O_3 were first grown from the V_2O_3 powder by the skull melting technique (*3*). These crystals were cut into thin slices with a thickness of 0.5 mm. These thin slices were then annealed at 1200°C under controlled oxygen partial pressure utilizing a mixture of CO and CO_2 gas to attain the desired composition of the specimens, which were then quenched to room temperature. The composition was determined by thermogravimetric analysis by reoxidizing the sample to V_2O_5. Equilibrium composition was assured by annealing the sample for 3 days. The compositions of six specimens are given in Table I. Specimen A has the stoichiometric composition, compositions of B and C fall into the region where the M–I transition temperature changes sharply, and compositions of D and E are close to the homogeneity limit which is reported to be $V_2O_{3.072}$ at 1227°C and $V_2O_{3.055}$ at 1127°C (*11*); although the exact composition of F was not determined, it was chosen to be outside the homogeneity range so that the V_2O_3 phase and the V_3O_5 phase coexist.

TABLE I

Sample	Composition	Annealing condition (at 1200°C)
A	$V_2O_{3.000}$	$\log P_{O_2} = -11.0$, 89 hr
B	$V_2O_{3.026}$	$\log P_{O_2} = -8.9$, 78 hr
C	$V_2O_{3.030}$	$\log P_{O_2} = -8.8$, 75 hr
D	$V_2O_{3.064}$	$\log P_{O_2} = -8.2$, 72 hr
E	$V_2O_{3.066}$	$\log P_{O_2} = -8.0$, 74 hr
F	—	$\log P_{O_2} = -7.7$, 24 hr

These crystals were crushed in an agate mortar and fine, crushed pieces were mounted on carbon films supported by copper grids for TEM observation. A JEM 200 CX with a side entry goniometer was used for observation.

Results of Observation

(i) Specimen A

The stoichiometric V_2O_3 crystal was investigated in detail first to gain background knowledge, so that features with respect to defects related to nonstoichiometry can be identified in nonstoichiometric crystals treated similarly.

Diffraction patterns obtained from all areas of specimen A showed clean Bragg spots of the corundum structure and no extra spots associated with a second phase or no diffuse scattering was found. In some areas, twins having a width of a few hundred angstroms and with boundaries paral-

lel to the $(0\bar{1}2)$ plane were observed. These twins are believed to be formed during crystal growth.

(ii) Specimens B and C

No particular difference with respect to microstructures between these two specimens could be detected. Both diffraction patterns and images from almost all areas from these specimens show the same characteristics as those of the stoichiometric specimen A. Twins were the only defects observed. However, in some areas of these specimens, image contrast due to the existence of a local strain was observed, and very weak extra diffraction spots were also observed in some diffraction patterns taken from the same areas. The existence of the heavy strain in the image indicates the existence of a second phase generated by precipitation or by transformation as explained below. However, these extra spots at this stage could not be identified with those of V_3O_5 or of any other known vanadium oxides. Because they are so weak that they cannot be seen on the fluorescent screen of the electron microscope, any detailed investigation with respect to the features of the diffraction spots is almost impossible. Except for the existence of the weak diffraction spots, no trace of diffuse scattering was detected even with long exposure times in obtaining diffraction patterns.

(iii) Specimens D and E

As in the case of specimens B and C, weak diffraction spots were detected in areas which show contrast due to the existence of heavy strain. In specimen E, a large particle of a second phase of about 1000 by 3000 Å was found (Fig. 1). The second phase is observed here as a part having moiré patterns, and its surroundings are heavily strained. Diffraction spots from this area were identified as those of V_3O_5. However, except from this particle, most extra spots from places showing heavy strain which are similar to that in Fig. 1 in specimens D and E are weak and cannot be explained on the basis of V_3O_5 or other known oxides of vanadium, as in the case of specimens B and C. The identification of the origin of these weak spots or the origin of the heavy strain is yet to be determined.

On the other hand, the existence of diffuse scattering was observed in these samples. Because the intensity of the diffuse scattering is so low, the observation has to be carried out very carefully. For example, if the thickness of the specimen is great, such diffuse scattering is almost unobservable because of the background due to inelastic scattering. If the orientation of the observed area corresponds to a low-index plane, the diffuse scattering is overwhelmed by strong Bragg spots (see Fig. 2c). However, if thin areas are selected and if the orientation deviates from that of low-index planes, diffuse scattering is clearly observed. In Fig. 2, these diffraction patterns in different orientations obtained from specimen D are shown. Figure 2e corresponds to the orientation in which no diffuse scattering is observed. Features of diffuse scattering from specimen E are the same as those from specimen D and are not shown here. The existence of diffuse scattering in nonstoichiometric V_2O_3 has not been previously reported.

The major feature of the diffuse scattering in these specimens is the existence of diffuse intensity plates perpendicular to the c^* axis located at $l = 3(2n + 1)$, where n is an integer. The plates are, however, not exactly flat, and characteristic curvatures of these plates with the period of the unit cell are found.

(iv) Specimen F

Observation indicated that most small particles obtained from specimen F are sin-

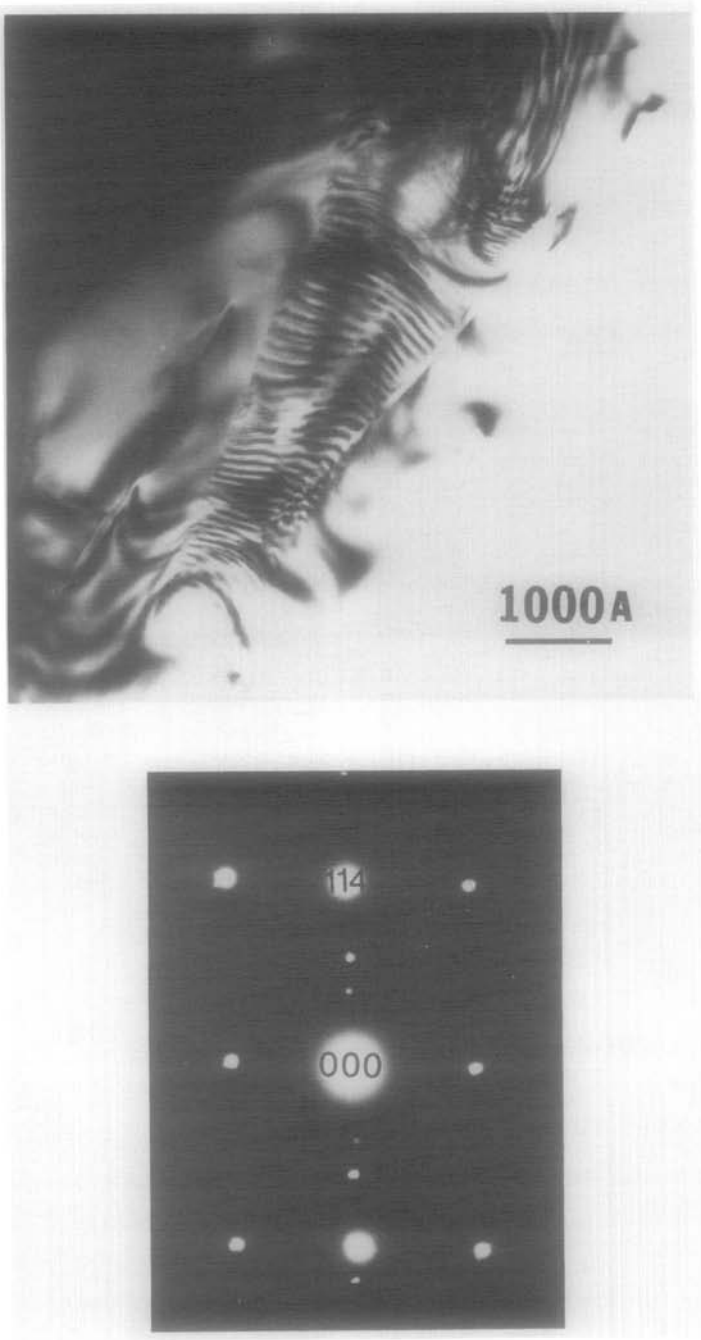

FIG. 1. A small precipitate of V_3O_5 observed in $V_2O_{3.066}$. The corresponding diffraction pattern is also shown.

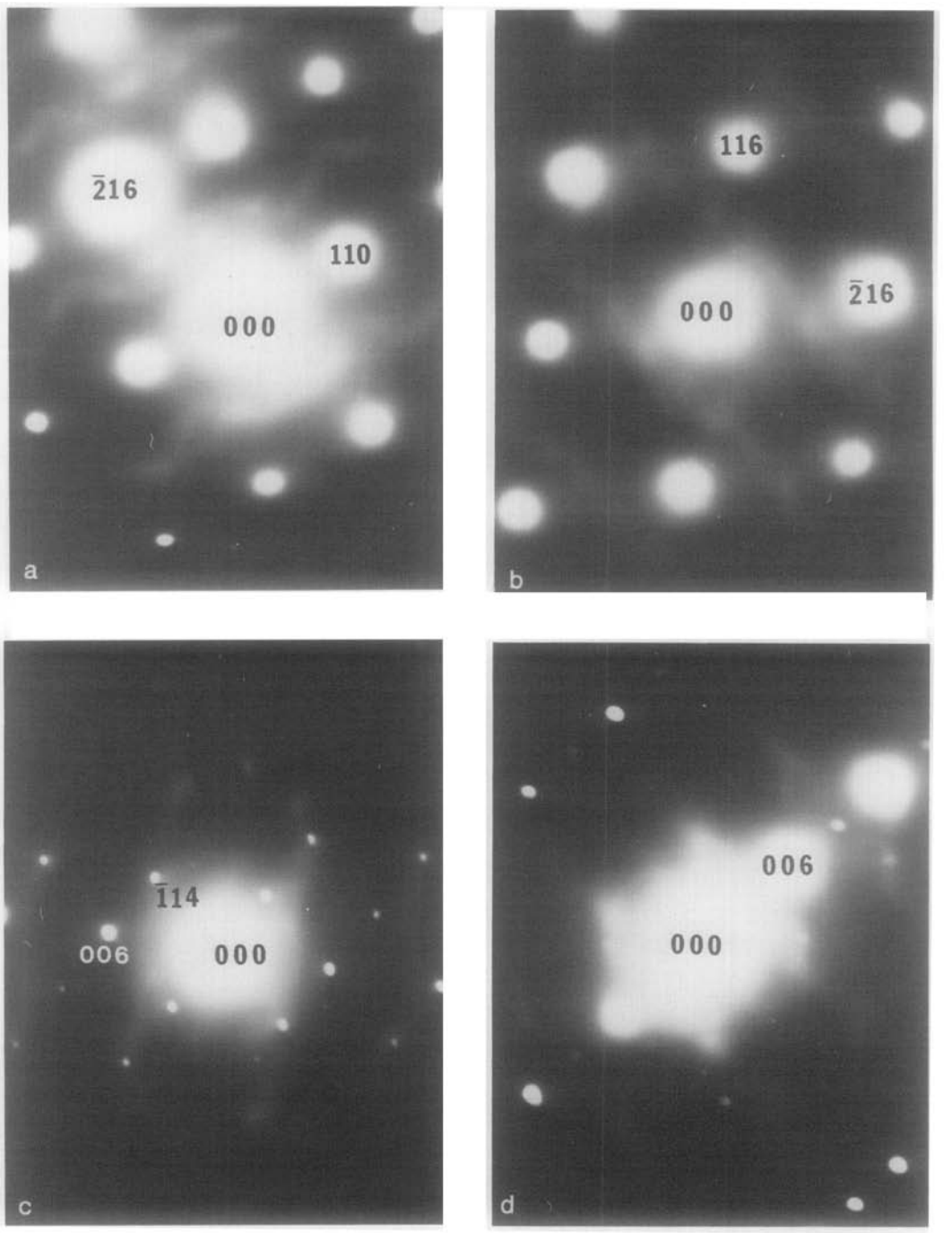

FIG. 2. Diffraction patterns taken from $V_2O_{3.094}$ indicating diffuse scattering. Beam orientations are (a) $[2\bar{2}1]$, (b) $[06\bar{1}]$, (c) [110], (d) [510], and (e) [001], respectively. (e) Corresponds to the orientation in which no diffuse scattering is observed.

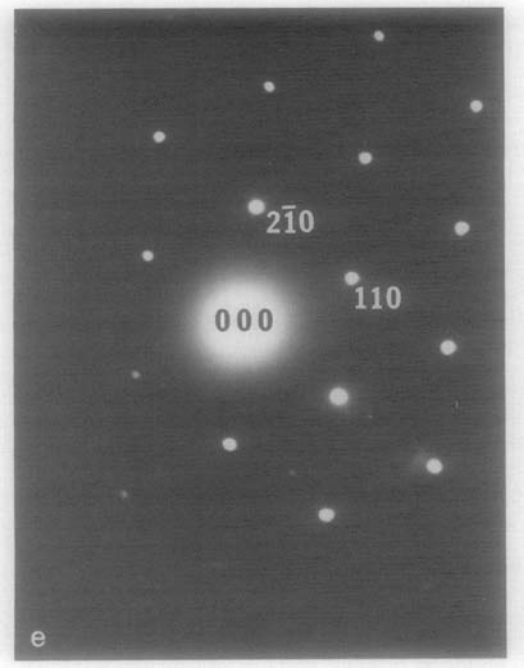

FIG. 2—*Continued.*

gle crystals of either V_2O_3 or V_3O_5. Some particles consist of two V_3O_5 grains with different orientations, indicating the decomposition of V_2O_3 into polycrystalline V_3O_5 by heat treatment. Some particles, on the other hand, consist of two phases. In Fig. 3, both the diffraction pattern and the bright-field image obtained from such a particle are shown. The image shows that the particle is sharply divided by a plane boundary. The corresponding diffraction patterns are indexed individually based on the structure of V_2O_3 and V_3O_5, respectively. The boundary is roughly normal to the image plane and is found to be parallel to the (1$\bar{1}$1) plane of V_2O_3 and to the (20$\bar{1}$) plane of V_3O_5. Based on the diffraction patterns, it can also be seen that the ($\bar{1}$14) plane and the [110] direction of the V_2O_3 crystal are parallel to the (100) plane and the [010] direction of the V_3O_5 crystal, respectively. Observations of other particles consisting of V_2O_3 and V_3O_5 show that the relative orientation of these two phases is always the same.

Crystal Structure of V_2O_3, V_3O_5, and VO_2

In order to discuss the effect of nonstoichiometry on local changes of structure with the change of composition of metal ions, it is advantageous to know the qualitative relations between the structures of those phases which can play a role. In the V–O system, distinct structures are determined basically by the distribution of V ions among the octahedral sites of the close-packed lattice formed by O^{2-} ions. In the following, we briefly discuss the essential features of these structures necessary for the later discussions.

(i) V_2O_3

At room temperature, V_2O_3 has the corundum-type structure with the space group $R\bar{3}c$. The oxygen ions form the close-packed hexagonal lattice ($2H$). The sublattice composed of octahedral interstitial sites is a simple hexagonal lattice with $c/a = 0.833$, assuming the ideal close-packed structure for the oxygen lattice. However, only two-thirds of the interstitial sites are occupied by V ions, and the distribution of vacant sites has threefold symmetry. In order to relate several structures in the same framework required for later discussions, we index the structure of V_2O_3 on the basis of the hexagonal lattice. Based on the hexagonal indexing, the lattice parameters of V_2O_3 are $a = 4.9492$ and $c = 13.998$ Å (*12*). Detailed atomic positions in connection with the M–I transition are given in Refs. (*12*) and (*13*).

(ii) VO_2

The crystal structure of VO_2 (the high-temperature phase) is that of rutile and belongs to the tetragonal lattice with the space group $P4_2/mnm$. However, if a small amount of distortion is disregarded, the lattice composed of oxygen ions is a close-packed hexagonal lattice and one-half of its octahedral sites are occupied by V ions.

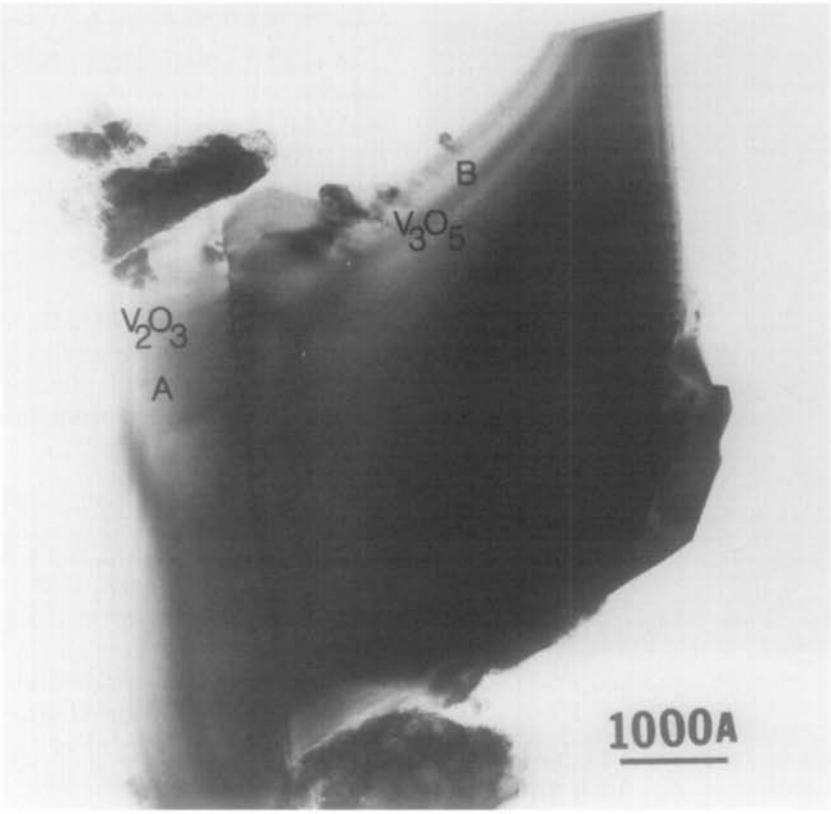

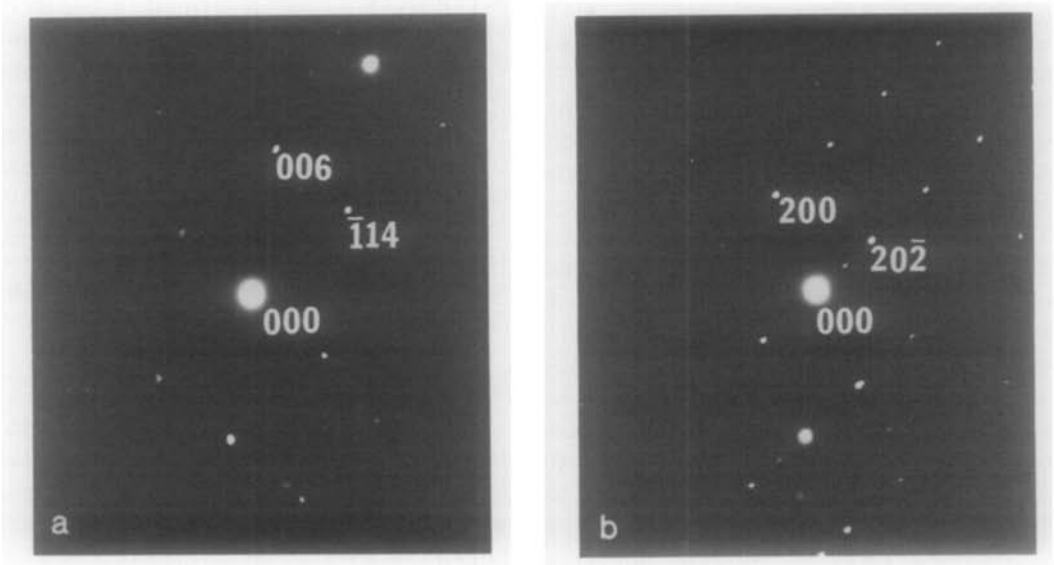

FIG. 3. Orientation relationships between V_2O_3 and V_3O_5 formed from V_2O_3 by heat treatment in an oxidizing atmosphere. (a) Bright-field image of V_2O_3 and V_3O_5 separated by a sharp boundary. (b) Diffraction patterns obtained from V_2O_3 and V_3O_5 of the same orientation as that in (a), showing the orientation relationship between these two parts.

This concept of the VO_2 structure is especially relevant in the present case in which the local deviation of the distribution of metal ions from the V_2O_3 structure is discussed. Indexing of the VO_2 structure is generally made based on the tetragonal, rutile structure. In this indexing, the c axis of the hexagonal (oxygen) lattice corresponds to the [010] axis, and the [110] and the [1$\bar{1}$0] axes of the hexagonal lattice correspond to the [10$\bar{3}$] axis and the [101] axis of the tetragonal rutile structure, respectively.

(iii) V_3O_5

A detailed structure of the room-temperature phase of V_3O_5 has been determined by Åsbrink (*14*). This belongs to the space group $P2/C$ with lattice parameters a = 9.859, b = 5.0416, c = 6.991 Å, and β = 109.478°.

Basically, V_3O_5 belongs to a homologous series of long-period compounds V_nO_{2n-1} ($3 \leq n \leq 9$), which is described as a periodic modulation of VO_2 by removing one oxygen layer at every nth V layer in the direction perpendicular to the (121) plane of VO_2 (*15*). Therefore, the structure of V_3O_5 is also closely related to VO_2 and can be described as a distribution of V ions in the octahedral sites of hexagonal close-packed oxygen lattice. The c axis of the hexagonal (oxygen) lattice corresponds to the [302] axis, and the [110] axis and the [1$\bar{1}$0] axis of the hexagonal lattice correspond to the [010] axis and the [10$\bar{1}$] axis, respectively, of the monoclinic V_3O_5 structure.

In Fig. 4, the arrangement of V ions among the interstitial sites of these three structures is compared for convenience in the following arguments utilizing the common hexagonal close-packed ($2H$) oxygen lattice. The locations of V ions are assumed to be exactly on the octahedral sites of the common oxygen lattice. Here, solid circles represent V ions and open circles represent the vacant sites in the equivalent orientation of these three different structures.

Analysis of the Diffuse Scattering

A major feature of the diffuse scattering is the existence of diffuse intensity plates in reciprocal space perpendicular to the c^* axis at the position $l = 3(2n + 1)$. Because the 006 reflection corresponds to the reciprocal spacing of the close-packed oxygen layers, this indicates the apperance of a new periodicity which is twice the distance of the spacing of the close-packed oxygen layer in the c direction.

It is, on the other hand, certain that this

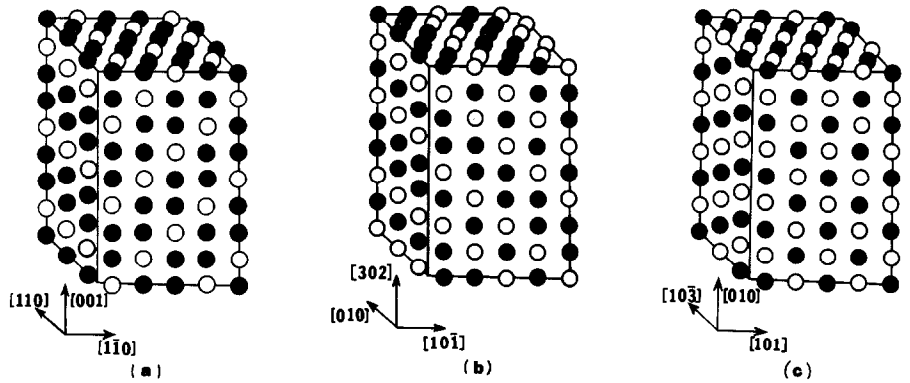

FIG. 4. Arrangement of V ions and vacant sites in the octahedral sites of an idealized hexagonal close-packed lattice in (a) V_2O_3, (b) V_3O_5, and (c) VO_2. Solid and open circles are metal ions and vacant sites, respectively.

appearance of diffuse scattering is caused by the change in the distribution of V ions by the increase in the number of vacant sites due to the nonstoichiometry. That this is due to the decrease in V ions by the increase in the number of vacant sites is corroborated by the fact that the increase in nonstoichiometry is accompanied by a decrease in the lattice parameters in both the c and a directions (*2, 16, 17*). Therefore, the appearance of the diffuse intensity plates perpendicular to the c^* direction is the result of the appearance of clusters consisting of one dimensionally ordered chains parallel to the c axis, where V ions and vacant sites alternate in the c direction so that the period of distribution of V ions is twice that of the spacing between the close-packed oxygen layers. This conclusion is based on the fact that the deviation from the stoichiometry is small and, hence, the density of clusters is also low. In such a case the diffuse scattering may simply be considered to be due to the superposition of scattered intensity from individual clusters.

The existence of curvature in the intensity distribution with the period of the unit cell indicates that there is some correlation in the phase of the ordering inside individual clusters with the period of the unit cell in the lateral direction. This indicates that the ordered regions or the clusters, although long in the c direction, consist of several chains with fixed phase relations among each other with the period of the basic lattice. A reasonable model to account for the observation is that the distribution of V ions in the lateral direction in the cluster is also that of VO_2. The resultant model of the clusters is shown in Fig. 5. In the Appendix, the calculation of the distribution of intensity in the reciprocal space based on this model is given. By assuming reasonable numbers with respect to the number of chains included in one cluster and to the length (the number, n, of octahedral sites included in a single chain), the calculation shows an intensity distribution which agrees well with the observation. In the calculation, the number of chains in the cluster is assumed to be three (forming a triangular column) or less and an average length of $\bar{n} = 6$ is assumed.

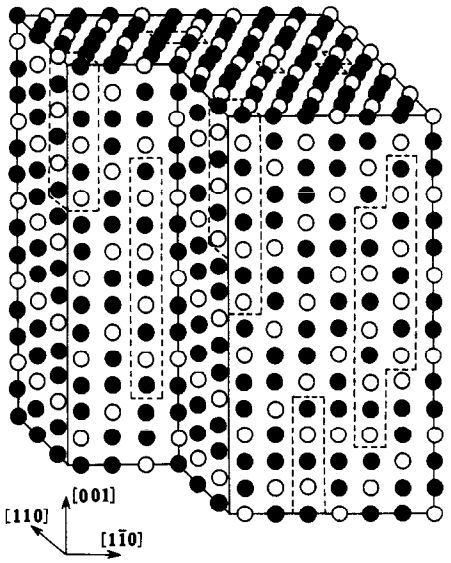

FIG. 5. Model of one-dimensional clusters in V_2O_3 which contribute to the diffuse scattering. Solid and open circles are metal ions and vacant sites, respectively. Oxygen atoms, which form the close-packed hexagonal lattice, are not shown.

Orientation Relationship between V_2O_3 and V_3O_5

Observation of specimen F shows that whenever V_2O_3 and V_3O_5 coexist, there also exists a certain orientation relationship between them. This indicates a transformation of V_2O_3 into V_3O_5 as the V content is decreased by the heat treatment. In Fig. 6, the relationship between V_2O_3 and V_3O_5 as indicated by the diffraction pattern in Fig. 3a is shown schematically. The boundary plane is normal to the projection plane and is indicated by a dotted line. It is seen that the close-packed layers of oxygen ions are common to both phases. The only change is

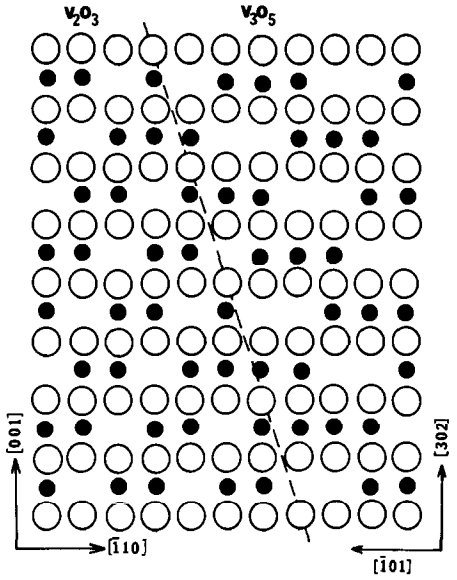

FIG. 6. Schematic orientation relationship between V_2O_3 and V_3O_5 shown in Fig. 3. Open circles represent oxygen ions and solid circles indicate metal ions.

the period of the arrangement of V ions. This situation indicates that the transformation from V_2O_3 to V_3O_5 is generated by the redistribution of V ions and vacancies on the octahedral interstitial sites due to the decrease in the density of V ions; the clustering (as indicated by the diffuse scattering) serves as the nucleus for the redistribution. A small nucleus of a V_3O_5 crystal observed in V_2O_3 (found in specimen E) in Fig. 1 has the same orientation relationships with the matrix as that presented here and is considered to be the transition stage between the clustering and the macroscopic precipitate. Heavily strained areas observed in specimens B, C, D, and E thus seem to be attributable to the pseudomorphic strain at the initial stage of precipitation. The orientation relationship shown in Fig. 6 is highly idealized. The actual location of ions and their relationship in both phases is shown in Fig. 7 in the same orientation. Numbers shown here indicate the positions of ions along the projection direction.

Discussion

A TEM study of V_2O_{3+x} in the range from $x = 0$ to $x = 0.066$ and beyond was made in order to investigate the effect of nonstoichiometry in V_2O_3. The result more or less corroborates the study of the phase diagram of the system; the homogeneity range extends to $x \cong 0.07$, and beyond this range V_2O_3 and V_3O_5 coexist. Although indications of the existence of a minor amount of precipitates are found in specimens of other than the stoichiometric composition, the relation between this finding and the limit of the homogeneity range is not sought. Beyond the composition $x \cong 0.06$, the existence of diffuse scattering becomes distinct. The analysis of the diffuse scattering indicates chainlike clustering whose structure is similar to that of VO_2, with the chains oriented along the c direction of the V_2O_3 matrix. Beyond the homogeneity limit, the coexistence of V_2O_3 and V_3O_5 is confirmed. In such cases, V_2O_3 and V_3O_5 show a definite mutual orientation and the close-packed oxygen ion layers of both phases may be considered to be in common. The situation thus corroborates the previous statement that several different phases in this system correspond to different ordered phases with respect to vanadium ions and vacancies depending on the concentration of vanadium ions on the octahedral sites of the common hexagonal close-packed lattice composed of oxygen ions.

The appearance of diffuse scattering in nonstoichiometric oxides having the rock salt structure, such as VO, TiO, and FeO, has been investigated extensively and has been attributed to a clustering which is a forerunner of the ordered phase with respect to metal ions and vacancies among octahedral and tetrahedral sites of the close-packed cubic oxygen sublattice at low temperatures. In this sense, the diffuse scattering which appears in the V_2O_{3+x} has a similar meaning to that which appears in

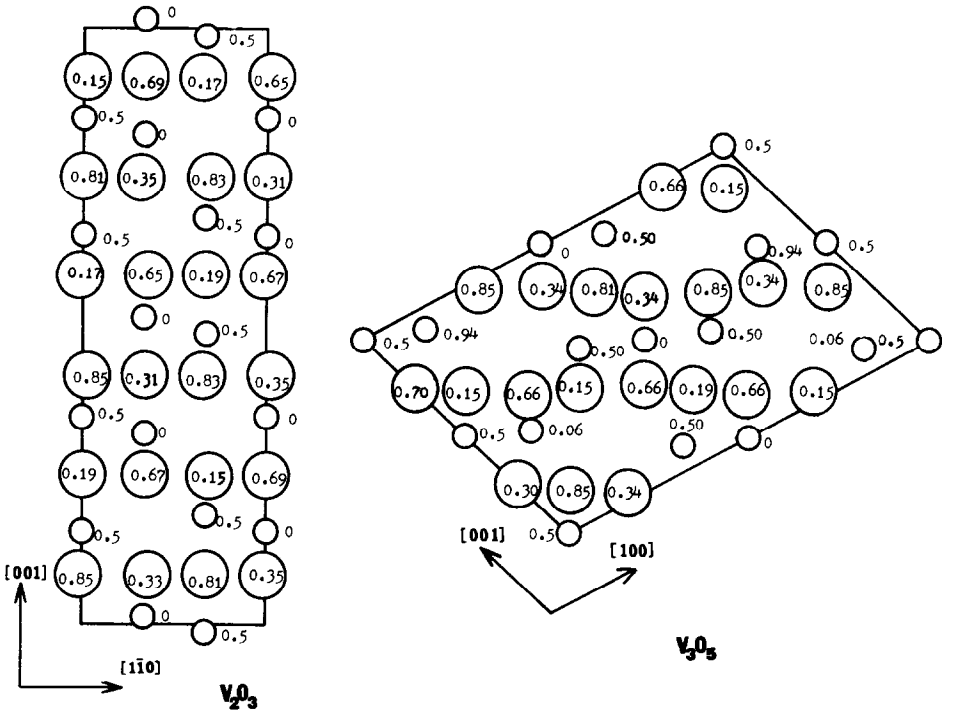

FIG. 7. Projection of V_2O_3 and V_3O_5 unit cells in the same orientation as that of Fig. 6. Large and small circles are oxygen and metal ions, respectively. Numbers shown indicate positions of ions along the direction of the projection.

the MO_{1+x} (M indicates a metal ion). The difference between these two is that, in the latter, the order–disorder of metal ions and vacancies with respect to temperature with a fixed metal ion concentration is usually treated, while in the former, the appearance of different ordered phases by the change of concentration of metal ions is the major problem. Experimentally, however, in the present case, a very small deviation from stoichiometry has to be considered and, hence, the detection of diffuse scattering is far more difficult. Indeed, the existence of diffuse scattering in V_2O_{3+x} had not been reported so far.

The origin of the diffuse scattering in V_2O_{3+x} is found to be clusters due to chainlike ordering of V ions and vacant sites whose structure is similar to VO_2 in the c direction. However, the structure of V_nO_{2n-1} to which V_3O_5 belongs can be considered to be derived by a periodic modulation of VO_2, and hence local ordering of metal ions and vacant sites in V_nO_{2n-1} is similar to that of VO_2. As long as the ordering is short range, it is hard to distinguish the structure of V_nO_{2n-1} and VO_2. In this sense, the clustering of vacancies near the phase boundary can be considered as the forerunner of the precipitation of V_3O_5. Usually, the structure of V_nO_{2n-1} is explained as the periodic modulation of VO_2 by removing an oxygen layer at every nth layer in the direction perpendicular to the (121) plane of VO_2. Although readily visualizable, this concept is sometimes misleading. In view of the fact that V_2O_3, V_3O_5, and VO_2 can be considered as differnt types of ordered phases with respect to V ions and vacant sites among interstitial sites of

the common close-packed oxygen lattice, it should rather be stated that the V_nO_{2n-1} phases represent long-period modulations of the ordered structure of metal ions and vacant sites of VO_2.

The direction of ordering in the cluster is predominantly in the c direction. This is presumably because the distance between metal ions in the c direction is shorter, and hence the correlation in the c direction is stronger. The ratio of the distance between metal ions on octahedral sites in the c and in the a direciton is 0.833 for the ideal hexagonal close-packed lattice.

The M–I transition temperature in V_2O_{3+x} depends very strongly on x and vanishes at $V_2O_{3.027}$. At this composition range, the existence of clusters is not appreciable although their existence cannot be denied. In this respect, it seems safe to conclude that the change of the M–I temperature in V_2O_{3+x} is a characteristic of the homogeneous phase.

Measurements of lattice parameters show that both a and c decrease linearly with the increase of x, indicating that vacant sites created by nonstoichiometry are distributed randomly among available octahedral sites (*2*, *16*, *17*). However, a measurement by Nakahira *et al.* (*16*) shows the interesting feature that, near the phase boundary, the parameter a decreases more rapidly while the parameter c remains at an almost constant value. This type of change reflects the appeaarance of an appreciable amount of clustering near the phase boundary. On the other hand, a recent detailed measurement of the composition dependence of fugacity of oxygen (*3*) does not reflect such a change. Presumably, thermodynamic properties such as fugacity depend mainly on the composition (number of vacancies) and is rather insensitive to minor changes of local arrangement, such as the clustering of vacancies on a small scale compared to those physical properties such as the lattice parameters.

Appendix: Calculation of the Intensity Distribution of Diffuse Scattering

The purpose of this calculation is to show how the structural model proposed for clusters in Fig. 5 can reproduce main features of the observed diffuse scattering. Two effects are excluded from the calculation for the sake of simplicity: one is the dynamical diffraciton effect and the other is the atomic displacement effect including thermal motions. It is assumed that oxygen ions form an ideal close-packed hexagonal lattice and each metal atom is located exactly at the center of its octahedral site.

First, the crystal is supposed to contain N clusters. We introduce functions $P(\mathbf{r}_j)$ and $P_k(\mathbf{r}_j)$ which define metal atom positions in structures of V_2O_3 and VO_2, respectively. If an octahedral site whose position is defined by a vector $\mathbf{r}_j$ is occupied by a metal atom, then

$$P(\mathbf{r}_j) = 1,$$

$$P_k(\mathbf{r}_j) = 1,$$

and if it is vacant, then

$$P(\mathbf{r}_j) = 0,$$

$$P_k(\mathbf{r}_j) = 0.$$

By using these functions, the total diffraction amplitude from the crystal is written as

$$R(\mathbf{q}) = f_M \sum_{\mathbf{r}_j}{}' P(\mathbf{r}_j)\exp(-2\pi\mathbf{q}\cdot\mathbf{r}_j) + f_M \sum_{k=1}^{N} \sum_{\mathbf{r}_j}{}^{(k)} P_k(\mathbf{r}_j)\exp(-2\pi i\mathbf{q}\cdot\mathbf{r}_j) + f_O \sum_{\mathbf{r}_j'} \exp(-2\pi\mathbf{q}\cdot\mathbf{r}_j'), \quad \text{(A1)}$$

where $\mathbf{q}$ is the scattering vector, f_M and f_O are the scattering factors for vanadium and oxygen ions, respectively, and a vector $\mathbf{r}_j'$ defines a position of the site for an oxygen atom. In Eq. (A1), the summation in the first term is made over the matrix excluding

clusters, the summation $\Sigma^{(k)}$ in the second term runs over the kth cluster, and the summation in the third terms is made over the whole crystal. Equation (A1) is then rewritten as

$$R(\mathbf{q}) = f_M \sum_{\mathbf{r}_j} P(\mathbf{r}_j)\exp(-2\pi i\mathbf{q}\cdot\mathbf{r}_j) + f_O \sum_{\mathbf{r}'_j} \exp(-2\pi i\mathbf{q}\cdot\mathbf{r}'_j) + f_M \sum_{k=1}^{N} \sum_{\mathbf{r}_j}^{(k)} (P_k(\mathbf{r}_j) - P(\mathbf{r}_j))\exp(-2\pi\mathbf{q}\cdot\mathbf{r}_j) \quad \text{(A2)}$$

where the summation of the first term is made over the entire matrix and other summations are carried out in the same way as in Eq. (A1). The first and second term in Eq. (A2) correspond to the diffraction amplitude from the V_2O_3 crystal without defect clusters, and the third term is attributed to that of clusters. If these two parts are represented as R_1 and R_2, the total diffraction intensity is written as

$$I = R_1R_1^* + R_1R_2^* + R_1^*R_2 + R_2R_2^*. \quad \text{(A3)}$$

In Eq. (A3), the first three terms give rise to fundamental reflections and diffuse scattering is given by the fourth term, which is written as

$$I_d = f_M^2 \left| \sum_{k=1}^{N} \sum_{\mathbf{r}_j}^{(k)} (P_k(\mathbf{r}_j) - P(\mathbf{r}_j))\exp(-2\pi i\mathbf{q}\cdot\mathbf{r}_j) \right|^2. \quad \text{(A4)}$$

Since interference effects between different clusters may be disregarded in the present case, the deviation from stoichiometry being small, Eq. (A4) may be rewritten

$$I_d = f_M^2 \sum_{k=1}^{N} \left| \sum_{\mathbf{r}_j}^{(k)} (P_k(\mathbf{r}_j) - P(\mathbf{r}_j))\exp(-2\pi i\mathbf{q}\cdot\mathbf{r}_j) \right|^2. \quad \text{(A5)}$$

For actual calculations, the model is further simplified as follows: first, it is assumed that the length of clusters is given by the number n of octahedral sites along the c axis and its distribution is assumed to be given by the Gaussian distribution function

$$W(n) = \frac{1}{(2\pi\sigma)^{1/2}} \exp\left\{-\frac{(n-\bar{n})^2}{2\sigma^2}\right\}, \quad \text{(A6)}$$

where $\bar{n}$ is the mean value of n, and σ is the dispersion factor.

Second, clusters are assumed to be classified into three groups only: the first group consists of only one chain of octahedral sites, the second group consists of two chains which are next to each other, and the third group consists of three chains which are next to each other and form an equilateral triangular rod. For clusters consisting of two or three chains, the relative arrangements of metal ions and vacant sites is assumed to be that of VO_2. The ratio of numbers of clusters belonging to the first, second, and third group is tentatively assumed to be 3 : 2 : 1.

Under these simplifications, the calculation of Eq. (A5) is now reduced to the superposition of scattering from microdomains of all possible groups with all possible orientations and distributions of metal ions whose lengths are determined by Eq. (A6). In Table II, values of $P_k(\mathbf{r}_j)$ and $P(\mathbf{r}_j)$ for a cluster consisting of three chains with $n = 8$ are shown as an example. Here, x_j, y_j and z_j are components of a vector $\mathbf{r}_j$ and $P_k(\mathbf{r}_j)$ is for the distributions of metal ions having the structure of VO_2 and $P(\mathbf{r}_j)$ is for that of V_2O_3.

The calculation is carried out for intensity distributions on various reciprocal lattice planes with different values of $\bar{n}$ and σ. Figure 8 is the calculated intensity distribution on the reciprocal lattice plane $(2\bar{2}1)^*$, $(061)^*$, and $(110)^*$, in arbitrary units. Values of $\bar{n}$ and σ are assumed to be 6 and 2, respectively. These intensity distributions should be compared with the diffraction

TABLE II

$P_k(\mathbf{r}_j)$ AND $P(\mathbf{r}_j)$ OF A DEFECT CLUSTER CONSISTING OF THREE CHAINS (n = 8)

	$P_k(\mathbf{r}_j)$ (x_j, y_j)			$P(\mathbf{r}_j)$ (x_j, y_j)		
z_j	Chain 1 (0.0)	Chain 2 (2/3, 1/3)	Chain 3 (1/3, 2/3)	Chain 1 (0.0)	Chain 2 (2/3, 1/3)	Chain 3 (1/3, 2/3)
0	0	1	0	0	1	1
1/6	1	0	1	1	0	1
2/6	0	1	0	1	1	0
3/6	1	0	1	0	1	1
4/6	0	1	0	1	0	1
5/6	1	0	1	1	1	0
6/6	0	1	0	0	1	1
7/6	1	0	1	1	0	1

patterns shown in Figs. 2a, b, and c. It can be seen that the main features of diffuse scattering are satisfactorily reproduced by the calculation. There are diffuse scattering bands at l = 3, while no appreciable diffuse scattering at l = 0 or 6 is found. Furthermore, these bands have curvatures similar to the observed ones. Curvatures of the cal-

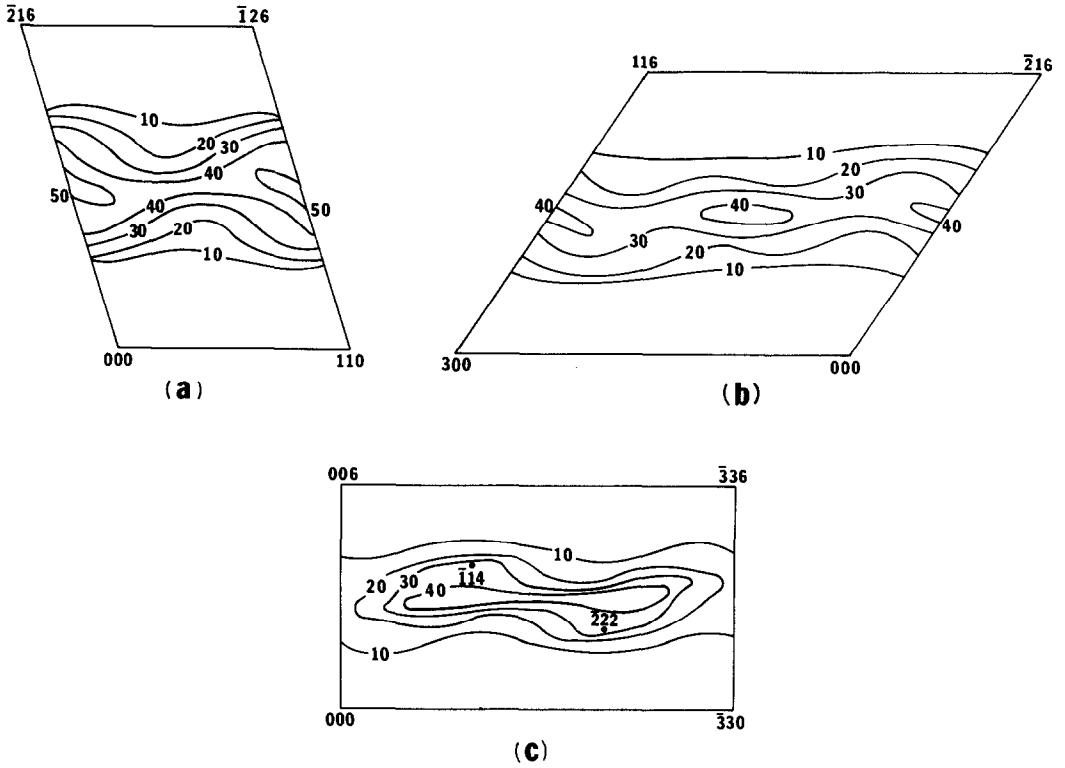

FIG. 8. Calculated intensity distribution of the diffuse scattering on (a) $(2\bar{2}1)^*$, (b) $(06\bar{1})^*$, and (c) $(110)^*$ planes.

culated distributions on the $(2\bar{2}1)^*$ and $(06\bar{1})^*$ coincide well with observed ones, although they are slightly shifted against each other along the $[110]^*$ direction on the $(2\bar{2}1)^*$ plane. On the other hand, the calculated distribution on the $(110)^*$ has a shape appreciably different from the observed one; the observed intensity distribution is shifted toward the high-angle side from the position defined by $l = 3(2n + 1)$. These discrepancies are presumably attributable to simplifications made for the model adopted.

It is difficult to derive quantitative information from diffuse scattering observed in electron diffraction patterns. However, it is found that observed features were reproduced most adequately for the value of $\bar{n}$ between 5 and 8. These values correspond to the length between 12 and 19 Å.

Acknowledgments

Helpful discussions with Dr. S. A. Shivashankar are highly appreciated. We also thank Mr. C. J. Sandberg for his help in preparation of specimens. This work was supported by NSF MRL Grant DMR-77-23798. Equipment provided through NSF Grants DMR-78-09025 and DMR-79-11137 was crucial for the success of this work.

References

1. J. M. Honig and L. L. Van Zandt, *in* "Annual Review of Materials Science, Vol. 5" (R. A. Huggins, R. H. Bube, and R. W. Roberts, Eds.), p. 225, Annual Reviews, Palo Alto (1975).
2. Y. Ueda, K. Kosuge, and S. Kachi, *J. Solid State Chem.* **31**, 171 (1980).
3. S. A. Shivashankar, R. Aragón, H. R. Harrison, C. J. Sandberg, and J. M. Honig, *J. Electrochem. Soc.* (1981).
4. L. Eyring and M. O'Keefe (Eds.), "The Chemistry of Extended Defects in Non-metallic Solids," North-Holland, Amsterdam (1970).
5. M. S. Seltzer and R. I. Jaffee (Eds.), "Defects and Transport in Oxides," Plenum, New York (1973).
6. H. Terauchi and J. B. Cohen, *Acta Crystallogr. Sect. A* **35**, 646 (1979).
7. B. Andersson, J. Gjonnes, and J. Tafto, *Acta Crystallogr. Sect. A* **30**, 216 (1974).
8. M. Morinaga and J. B. Cohen, *Acta Crystallogr. Sect. A* **35**, 975 (1979).
9. F. Koch and J. B. Cohen, *Acta Crystallogr. Sect. B* **25**, 275 (1969).
10. A. K. Cheetham, B. E. F. Fender, and R. I. Taylor, *J. Phys. C* **4**, 2160 (1971).
11. M. Wakihara and T. Katsura, *Metal. Trans.* **1**, 363 (1970).
12. W. Robinson, *Acta Crystallogr. Sect. B* **31**, 1153 (1975).
13. P. D. Dernier, *J. Phys. Chem. Solids* **31**, 2569 (1970).
14. S. Åsbrink, *Acta Crystallogr. Sect. B* **36**, 1332 (1980).
15. S. Anderson and L. Jahnberg, *Ark. Kemi* **21**, 413 (1963).
16. M. Nakahira, S. Horiuchi, and H. Ooshima, *J. Appl. Phys.* **41**, 836 (1970).
17. D. B. McWhan, A. Menth, and J. P. Remeika, *J. Physique* **31**, *C* 1-1079 (1971).